

## Key Atmospheric Signatures for Identifying the Source Reservoirs of Volatiles in Uranus and Neptune

O. Mousis · A. Aguichine · D. H. Atkinson ·  
S. K. Atreya · T. Cavalié · J. I. Lunine ·  
K. E. Mandt · T. Ronnet

Received: date / Accepted: date

**Abstract** We investigate the enrichment patterns of several delivery scenarios of the volatiles to the atmospheres of ice giants, having in mind that the only well constrained determination made remotely, i.e. the carbon abundance measurement, suggests that their envelopes possess highly supersolar metallicities, i.e. close to two orders of magnitude above that of the protosolar nebula. In the framework of the core accretion model, only the delivery of volatiles in solid forms (amorphous ice, clathrates, pure condensates) to these planets can account for the apparent supersolar metallicity of

---

O. Mousis  
Aix Marseille Univ, CNRS, CNES, LAM, Marseille, France  
Tel.: +33-491-055-918  
Fax: +33-491-621-190  
E-mail: olivier.mousis@lam.fr

A. Aguichine  
Aix Marseille Univ, CNRS, CNES, LAM, Marseille, France

D. H. Atkinson  
Jet Propulsion Laboratory, California Institute of Technology, 4800 Oak Grove Dr., Pasadena, CA, 91109, USA

S. K. Atreya  
Department of Climate and Space Sciences and Engineering, University of Michigan, Ann Arbor, MI 48109-2143, USA

T. Cavalié  
Laboratoire d'Astrophysique de Bordeaux, Univ. Bordeaux, CNRS B18N, allée Geoffroy Saint-Hilaire, 33615 Pessac, France

LESIA, Observatoire de Paris, PSL Research University, CNRS, Sorbonne Universités, UPMC Univ. Paris 06, Univ. Paris Diderot, Sorbonne Paris Cité, F-92195 Meudon, France

J. I. Lunine  
Department of Astronomy, Cornell University, Ithaca, NY 14853, USA

K. E. Mandt  
Applied Physics Laboratory, Johns Hopkins University, 11100 Johns Hopkins Rd., Laurel, MD 20723, USA

T. Ronnet  
Lund Observatory, Department of Astronomy and Theoretical Physics, Lund University, Box 43, 221 00 Lund, Sweden

their envelopes. In contrast, because of the inward drift of icy particles through various snowlines, all mechanisms invoking the delivery of volatiles in vapor forms predict subsolar abundances in the envelopes of Uranus and Neptune. Alternatively, even if the disk instability mechanism remains questionable in our solar system, it might be consistent with the supersolar metallicities observed in Uranus and Neptune, assuming the two planets suffered subsequent erosion of their H-He envelopes. The enrichment patterns derived for each delivery scenario considered should be useful to interpret future in situ measurements by atmospheric entry probes.

**Keywords** Uranus · Neptune · atmospheric probes · formation models · in situ measurements

## 1 Introduction

The ice giant planets Uranus and Neptune represent a largely unexplored class of planetary objects that bridges the gap between the larger gas giants and the smaller terrestrial worlds. Uranus and Neptune’s great heliocentric distances have made exploration challenging, being limited to flybys by the Voyager 2 mission in 1986 and 1989, respectively (Tyler et al. 1986; Lindal et al. 1987; Smith et al. 1986, 1989; Lindal 1992; Stone and Miner 1986, 1989). Hence, most of our knowledge of atmospheric processes taking place on these distant planets is derived from remote sensing measurements acquired from Earth-based observatories and space telescopes (Encrenaz 2000; Karkoschka and Tomasko 2009, 2011; Fletcher et al. 2010, 2014; Feuchtgruber et al. 2013; Orton et al. 2014a,b; Sromovsky et al. 2014; Lellouch et al. 2010, 2015; Irwin et al. 2018, 2019a,b). As a consequence, our knowledge of their bulk composition is dramatically limited, resulting in a very crude understanding of their formation conditions and evolution (Atreya et al. 2020).

To improve this situation, ground-truth measurements carried out in these distant planets by an atmospheric probe are needed, similar to the Galileo probe at Jupiter. Remote observations cannot provide direct, unambiguous measurements of the vertical atmospheric structure (temperatures and winds), bulk composition and cloud properties. The well-mixed atmosphere for measuring the bulk composition, hence the elemental abundances, is much deeper than the deepest levels ( $\sim 1$  bar) reached by remote sensing measurements (Atreya et al. 2020). With the exception of  $\text{CH}_4$  (Karkoschka and Tomasko 2009, 2011; Sromovsky et al. 2011), and to some extent  $\text{H}_2\text{S}$  (Irwin et al. 2018, 2019a,b), remote observations have never been able to detect the key volatile species ( $\text{NH}_3$ ,  $\text{H}_2\text{O}$ ) thought to compose the deep ice giant clouds. Also, noble gases are out of reach of remote sensing measurements. This is an important issue because these species provide extremely important insights concerning the formation and evolution conditions of the solar system bodies (Pepin 1991; Owen et al. 1999; Gautier et al. 2001; Marty et al. 2017; Mandt et al. 2015; Mousis et al. 2009a, 2019) (see also Mandt et al. (2020), this issue). In the meantime, both NASA and ESA agencies are expressing their interest in sending of a joint flagship mission in the 2030s that would include an atmospheric entry probe as an element of a larger orbiter to be dropped toward the ice giants (see Simon et al. (2020), this issue). In this context, the aim of this paper is to review the different delivery scenarios of the volatiles to the ice giants and to derive the corresponding fingerprints in their atmospheres. The measurements of such fingerprints by atmospheric entry probes would pose important constraints on the formation scenarios of Uranus and Neptune.

Section 2 is dedicated to a brief summary of the known atmospheric abundances in both Uranus and Neptune. In Section 3, we review the different scenarios of volatiles delivery proposed in the literature and that can be applied to the ice giants. We also investigate further a mechanism of radial drift/diffusion for the main volatiles of interest ( $\text{H}_2\text{O}$ ,  $\text{CO}$ ,  $\text{N}_2$ ,  $\text{H}_2\text{S}$ ,  $\text{Ar}$ ,  $\text{Kr}$ , and  $\text{Xe}$ ) around their respective snowlines in the protosolar nebula (PSN). This mechanism has already been used to explain the distribution of volatiles throughout the protosolar nebula (Stevenson and Lunine 1988; Cyr et al. 1998, 1999; Ali-Dib et al. 2014; Mousis et al. 2019). Section 4 is devoted to the inference of the atmospheric fingerprints for each of the considered scenarios of volatiles delivery. Section 5 is dedicated to discussion and conclusions.

## 2 Atmospheric Abundances

Figure 1 shows the elemental abundance ratios in the giant planets relative to those in the proto-Sun, based on the values listed in Table 1 (see Atreya et al. (2019) for details). For Uranus and Neptune, only the C/H has been directly determined from the analysis of Voyager radio occultation and Hubble Space Telescope data, respectively. The C/H ratio on these planets is inferred to be  $80 \pm 20 \times$  solar, but is uncertain as it involves assumptions about the amount of H tied up in non-methane volatiles, whose abundances are unknown (see Atreya et al. (2020), this issue, for details).  $\text{NH}_3$  and  $\text{H}_2\text{S}$  would be expected to be significantly enriched relative to solar values, much like the observed enrichment in  $\text{CH}_4$ , assuming that the building blocks of Uranus and Neptune have solar C/N and C/S. Furthermore, S/N should also be solar, which would predict a value of  $\sim 0.2$ .

However, ground-based observations have measured ammonia in the atmospheres of Uranus and Neptune since the late 1970's. Gulkis et al. (1978) found that unlike Jupiter and Saturn,  $\text{NH}_3$  is subsolar by a factor of 100 at temperatures below 250 K (pressures  $< 40$  bars) in the observable atmospheres of these planets. This finding was later confirmed by Very Large Array (VLA) observations of radio emission spectra from Uranus and Neptune over the wavelength interval from  $\sim 0.1$  to 20 cm, corresponding to pressures down to  $\sim 50$  bars (de Pater et al. 1989, 1991). At the wavelengths considered, the opacity from  $\text{NH}_3$  is important enough, compared with those from  $\text{H}_2\text{O}$  and  $\text{H}_2\text{S}$ , to derive a subsolar  $\text{NH}_3$  abundance in Uranus and Neptune. The observed depletion of  $\text{NH}_3$  cannot be a consequence of condensation of this species, which is expected to occur at much shallower levels. The depletion of ammonia manifests itself in the presence of  $\text{H}_2\text{S}$  in the upper tropospheres of Uranus and Neptune. This is due to the fact that in thermochemical models of the giant planets  $\text{NH}_3$  serves as a sink for  $\text{H}_2\text{S}$  by forming a cloud of ammonium hydrosulfide. With little ammonia available,  $\text{H}_2\text{S}$  vapor can survive. In fact,  $\text{H}_2\text{S}$  vapor has now been detected on both Uranus and Neptune (Irwin et al. 2018, 2019a). With  $\text{S/N} \geq 5$ , an  $\text{H}_2\text{S}$  ice would form at 3 bars or deeper. The presence of an opacity source in this pressure region was inferred from the VLA data (de Pater et al. 1989, 1991). These observations appear to suggest non-solar C/N and S/N abundance ratios in the Ice Giants that may be tracers of building blocks that were also non-solar (Mandt et al. 2019). It should be stressed however that although  $\text{NH}_3$  and  $\text{H}_2\text{S}$  have been detected in the tropospheres of Uranus and Neptune, their bulk abundances are unknown. It is possible that the  $\text{NH}_3$  could be removed in a purported water ocean at the 10-kilobar level or deeper, and possibly an ionic ocean at 100 kilobars and deeper (see Atreya et al. (2020), this issue, for details of cloud

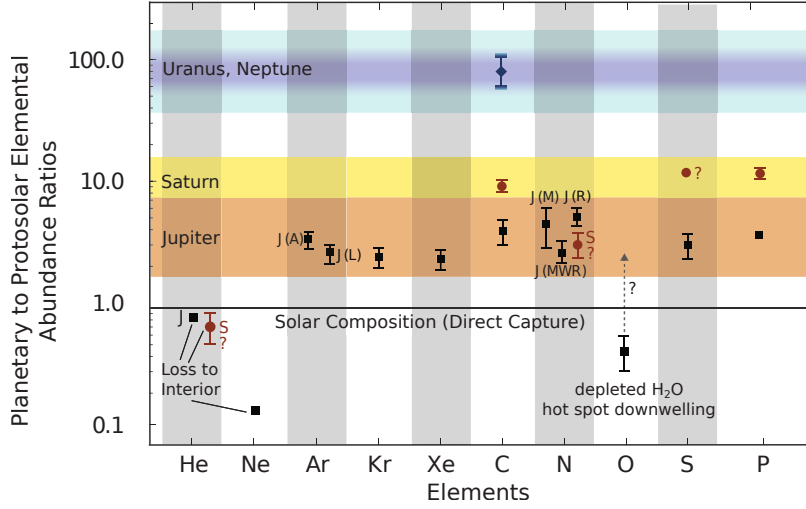


**Fig. 1** Elemental abundance ratios in the atmospheres of Jupiter, Saturn, Uranus and Neptune. “N” in Jupiter represents values from ammonia ( $\text{NH}_3$ ) abundance measurements made by the Galileo probe (mass spectrometer: [J(M)] and attenuation of probe radio signal: J[R]) and the Juno microwave spectrometer [J(MWR)], whereas “Ar” values are based on protosolar Ar/H values of Asplund et al. (2009) [J(A)] and Lodders et al. (2009) [J(L)]. Saturns He and N are labeled S. N/H of Saturn is a lower limit, and S/H is highly questionable. Only C/H is determined for Uranus and Neptune from ground-based  $\text{CH}_4$ , but remains uncertain. See Atreya et al. (2019) and references therein for all relevant details. [This version of the figure appears as Fig. 3 in Atreya et al. (2020), this issue, which was adapted from Fig. 2.1 of Atreya et al. (2019), with permission from Cambridge University Press, PLSclear Ref No: 18694].

structure and ammonia depletion). In other words, the question of the possible N and S depletions in the atmospheres of Uranus and Neptune remains open.

### 3 Scenarios of Volatiles Delivery

In this section, we depict the two main mechanisms of giant planet formation, i.e. the disk instability and core accretion models. In the first scenario, giant planets essentially grow from gas while, in the second scenario, their accretion requires the formation of a solid core before the accretion of gas and alternately solids. For each of these scenarios, we review and investigate the different delivery mechanisms of volatiles that can account for the volatiles enrichments observed in the ice giants atmospheres. Figure 2 summarizes the implications for the metallicity of the envelopes of Uranus and Neptune in the cases of the delivery mechanisms of volatiles discussed below.

#### 3.1 Disk Instability Model

One model for the formation of the giant planets posits the destabilization of the disk at an early stage in its evolution. Spiral density waves develop which transport angular momentum outward and mass inward, the latter allowing the self-gravity of the disk

**Table 1** Elemental abundance ratios in the Sun, Uranus and Neptune (this is a subset of Table 1 in Atreya et al. (2020))

Elements	Sun-Protosolar <sup>(a,b)</sup>	Uranus/Protosolar	Neptune/Protosolar
He/H	$9.55 \times 10^{-2}$	$0.94 \pm 0.16^{(c)}$	$1.26 \pm 0.21^{(c)}$ $0.94 \pm 0.16^{(c)}$
Ne/H	$9.33 \times 10^{-5}$	NA	NA
Ar/H	$2.75 \times 10^{-6}$	NA	NA
Kr/H	$1.95 \times 10^{-9}$	NA	NA
Xe/H	$1.91 \times 10^{-10}$	NA	NA
C/H	$2.95 \times 10^{-4}$	$80 \pm 20^{(d)}$	$80 \pm 20^{(e)}$
N/H	$7.41 \times 10^{-5}$	$0.01\text{--}0.001^{(f)}$	$0.01\text{--}0.001^{(f)}$
O/H	$5.37 \times 10^{-4}$	NA	NA
S/H	$1.45 \times 10^{-5}$	$> (\sim 0.4\text{--}1.0)^{(g)}$	$> (\sim 0.1\text{--}0.4)^{(h)}$
P/H	$2.82 \times 10^{-7}$	NA	NA

(a) Protosolar values based on the solar photospheric values of Asplund et al. (2009). (b) Protosolar metal abundances relative to hydrogen can be obtained from the present day photospheric values (Asplund et al. 2009), increased by +0.04 dex, i.e. 11%, with an uncertainty of  $\pm 0.01$  dex; the effect of diffusion on He is very slightly larger: +0.05 dex ( $\pm 0.01$ ). (c) Gautier et al. (1995); two values are given for Neptune, one without N<sub>2</sub> in the atmosphere (larger He/H) and the other including N<sub>2</sub> in order to explain presence of HCN. (d) Sromovsky et al. (2011); E. Karkoschka and K. Baines, personal communication (2015). (e) Karkoschka and Tomasko (2011). (f) See text. (g) Irwin et al. (2018), (h) Irwin et al. (2019a); lower limit below an H<sub>2</sub>S cloud, based on the detection of H<sub>2</sub>S gas in the 1.2–3 bar region above the cloud. This S/H is not necessarily representative of the actual value in the deep well-mixed atmosphere (see text).

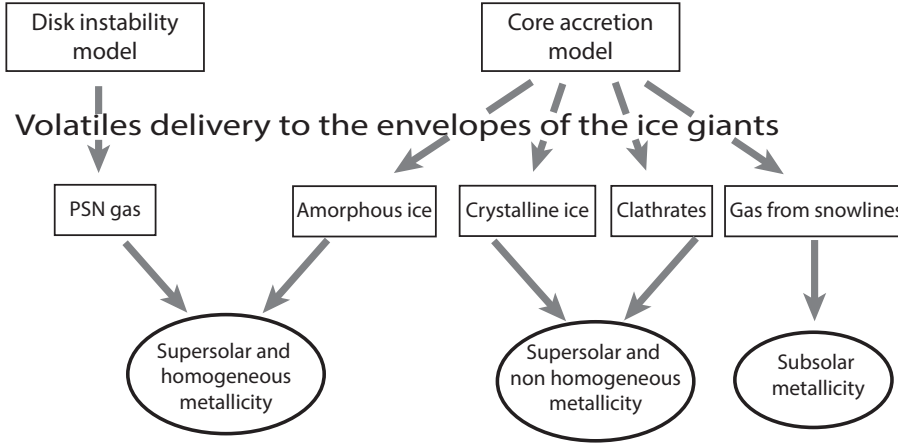


**Fig. 2** Metallicity of the envelopes of Uranus and Neptune derived for each of the considered delivery mechanisms of volatiles.

to tap into the free energy of the combined central protosun-disk system. A disk will become gravitationally unstable as the amplitude of the spiral density waves increases, if the disk is sufficiently massive and sufficiently cool (Armitage 2010). It will then break up into discrete mass concentrations which can continue to compact under their own self gravity, leading to a large number of giant planets (Boss 1997). The instability

mechanism is fast, leading to giant planet formation in hundreds to perhaps thousands of years (Mayer et al. 2004). Subsequent interaction with the disk can lead potentially to large enrichments of heavy elements, even large cores (Boley et al. 2011). Subsequent erosion of the H-He envelope might then produce something looking like an ice giant. Therefore, it may be difficult to use heavy-element composition to distinguish between core accretion and disk instability models since both cases predict significant volatile enrichments in the envelope.

However, it may be difficult for most disks to undergo the fragmentation required to generate giant planets even if the disk instability mechanism is at play. Extraction of gravitational potential energy as spiral density waves moves angular momentum outward and mass inward leading to heating of the disk, which tends to bring the disk away from the criterion of instability defined in Armitage (2010). The production of multiple giant planets in orbital relationships that are dynamically unstable leads to ejection of some planets and resulting placement of others on eccentric orbits that seem inconsistent with the architecture of the outer solar system. Mechanisms for post-fragmentation atmospheric enrichment that lead, for example, to the variation in enrichment seen in Jupiter have yet to be demonstrated. Finally, whether enough solid material remains to subsequently build the terrestrial planets, and even to populate the outer solar system with the initial reservoir of solid bodies that must be the source of the Oort Cloud and primordial Kuiper Belt, are open questions. The disk instability model cannot be ruled out as the operative mechanism for the formation of the giant planets, including Uranus and Neptune, but seems to raise more questions than it answers.

### 3.2 Core Accretion Model

In the core accretion scenario, the formation of giant planets starts with the build-up of a core, followed by the slow contraction of a gaseous envelope, and, if the envelope becomes massive enough, a phase of rapid, so-called runaway, gas accretion is eventually triggered (Pollack et al. 1996). Giant planets formation is then first dominated by the accretion of solids and later on, by the accretion of gas. In this respect, the bulk composition of Uranus and Neptune, with inferred metallicities in the range  $\sim 0.8$ – $0.9$  (Helled et al. 2011; Podolak et al. 2019), is indicative of the fact that these planets never reached the runaway gas accretion phase, or did so only towards the very end of the lifetime of the PSN, thus preventing them from becoming gas dominated planets like Jupiter and Saturn.

In details, the composition of the envelopes of Uranus and Neptune depends on their formation history, the size and composition of their building blocks, and the metallicity of the gas they accreted. The solids accreted by Uranus and Neptune could have either sunk to the center of the planets or been diluted in their envelope depending on their sizes (Podolak et al. 1988; Lozovsky et al. 2017). The formation timescale of Uranus and Neptune from large ( $> \text{km}$  sized) planetesimals would by far exceed the expected lifetime of the PSN (Levison and Morbidelli 2007; Levison et al. 2010). Instead, these planets most likely grew by accreting millimetre to centimetre sized drifting particles in a process known as pebble accretion (Lambrechts and Johansen 2012; Lambrechts et al. 2014). The pebbles are more likely to be diluted in the envelopes of the planets rather than to sink down to a core (Lambrechts et al. 2014; Chambers 2017; Brouwers et al. 2018). Also, contrary to large planetesimals whose composition is somewhat locked up

once they have formed, the volatile composition of the pebbles is expected to quickly adapt to the local temperature and pressure conditions of the disk, with condensation and evaporation taking place around the location of the so-called snowlines (Ros and Johansen 2013; Ali-Dib et al. 2014; Booth et al. 2017). Pebbles are also able to transport volatile species and noble gases that could have been trapped within the amorphous matrix of water ice (Mousis et al. 2019) or eventually in the form of clathrates. Finally, it should be noted that the high obliquities of Uranus and Neptune might be the result of violent impacts that took place during the final assembly of the ice giants (Morbidelli et al. 2012; Izidoro et al. 2015; Reinhardt et al. 2019). Such giant impacts could not only deliver some heavy elements to the envelope of the planets, but also substantially alter their interior and thus affect their long-term evolution (Reinhardt et al. 2019; Liu et al. 2019).

In this context, a long-standing debate is the question of the nature of the reservoirs of materials that contributed to the formation of giant planets, comets, and Kuiper-Belt Objects (Owen et al. 1999; Gautier et al. 2001; Bar-Nun et al. 2007; Rubin et al. 2015; Mousis et al. 2018). In the following, we describe the different delivery mechanisms of the volatiles to the forming giant planets in the framework of the core accretion model.

### 3.2.1 Amorphous Ice

The observed uniform enrichment in Jupiter in a class of heavy elements not affected by deep envelope miscibility (He, Ne) is puzzling, given that the original molecular carriers and the noble gases Ar, Kr, Xe have such widely varying volatilities. For example, in the case of carbon, the two major carriers CO and CH<sub>4</sub> vary in their vapor pressures at 40 K by three orders of magnitude. One scenario invoked in the literature to account for this homogeneous enrichment is the delivery of amorphous planetesimals to Jupiters envelope (Owen et al. 1999). The ratio of trapped volatiles to water in amorphous ice can be up to about 8%, depending on its porosity and surface available for adsorption (Schmitt et al. 1989). Figure 3 shows the release of gas from amorphous ice versus temperature derived from experiments depicted in Bar-Nun et al. (2007) for an initial deposition ratio of H<sub>2</sub>O:CO:N<sub>2</sub>:Ar = 100:100:14:1. Once the condensed ices of each species are sublimated below 60 K, a significant amount of CO and Ar are retained but very little N<sub>2</sub>. The result, if Jupiter was indeed seeded directly by amorphous planetesimals, might be a deficit of nitrogen unless ammonia was also present in sufficient amounts in the planetesimals. Also, a rather large water enrichment –at least similar to that of carbon– might result.

Owen et al. (1999) proposed that the planetesimals that seeded Jupiter were extremely cold, perhaps 30 K, so that the entire trapped volatile load seen in Figure 3 –directly condensed ices and that trapped in the amorphous water ice– could have been delivered to Jupiter. This would produce a more uniform enrichment, as observed, but would require very cold conditions at Jupiter. This scenario is more appropriate in the cases of Uranus and Neptune, which were located farther out in the protoplanetary disk and plausibly accreted very cold planetesimals. Assuming the two planets i) never reached the pebble isolation mass, which prevents the efficient accretion of centimeter- to meter-sized solids (Bitsch et al. 2018), and ii) the absence of larger planetesimals in the feeding zones, their growth from a mixture of gas and amorphous solids would lead to a uniform enrichment of heavy elements in their envelopes. If Uranus and Neptune exceeded the pebble isolation mass at the time their envelopes formed, one might expect a much more limited enrichment of heavy elements, but still uniform, unless

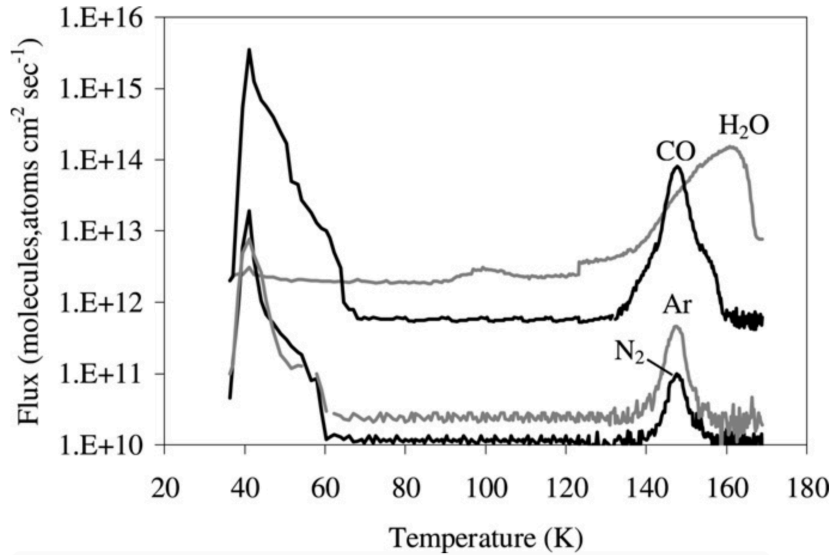


**Fig. 3** Flux of gases vs temperature in the experiments of Bar-Nun and colleagues. Low temperature (40–60 K) release is of pure ices sublimating off of grains. Release between 140–160 K is the conversion of amorphous to crystalline ice. [Figure 1 of Bar-Nun et al. (2007), with permission from Elsevier, XXX].

large planetesimals were dominant in the feeding zones. In this case, a substantial and uniform enrichment of heavy elements would be expected in the envelopes since the accretion of such planetesimals would not be affected by the pressure bump defining the pebble isolation mass (Bitsch et al. 2018). Either way, the signature of the accretion of amorphous solids would be the distinct difference in enrichment of water (hence, O) between the ice giants and Jupiter.

### 3.2.2 Crystalline Ices

When interstellar medium amorphous grains enter the PSN and cross the amorphous-to-crystalline transition zone (ACTZ), i.e. the zone within which the disk temperature reaches or exceeds  $\sim 143$  K (Bar-Nun et al. 2007), water ice crystallizes and the adsorbed volatiles are released to the disk gas phase. Because the PSN slowly cools down with time, the released volatiles will form crystalline ices whose condensation temperatures are lower than the one needed to crystallize amorphous ice. These crystalline ices can consist in pure condensates forming in a temperature range comprised between  $\sim 20$  and 150 K in the PSN, depending on their abundances relative to  $H_2$  and the equilibrium pressures of the considered species (see Fig. 4, top panel). Alternatively, crystalline ices can exist in the form of clathrates, which are ice-like inclusion compounds forming with nonpolar guest molecules surrounded with hydrogen-bonded water cages (Sloan and Koh 2008). The ratio of trapped volatiles to water in clathrates is up to about 1:6 total trapped gas (Sloan and Koh 2008). Clathrates typically crystallize in the PSN at higher temperatures than those of the pure condensate forms of their encaged molecules (Fig. 4, bottom panel). Clathrate formation essentially depends on the availability of



crystalline water ice in the PSN (Lunine and Stevenson 1985; Mousis et al. 2010), and also on the kinetics of entrapping, which remains to be assessed (Ghosh et al. 2019a,b; Choukroun et al. 2019). The building blocks of all giant planets of our solar system, as well as comets and Kuiper-belt objects, might have formed from one of these two kinds of crystalline ices, or maybe from a mixture of both.

Assuming formation at temperatures low enough to enable the crystallization of ultra-volatiles such as Ar or N<sub>2</sub> (see Fig. 4, top panel), planetesimals agglomerated from pure condensates should display a composition slightly different from the one derived from a protosolar mixture. Because the equilibrium temperatures of the considered ices vary over several dozens of kelvins, they are expected to condense at different epochs of the PSN evolution. As a result, the volatile A/volatile B abundance ratio in solid phase should be higher than the one derived from their gas phase abundances if volatile A crystallizes at a higher temperature than volatile B. This is due to the fact that the disk dissipates with time, implying a continuous decrease of its surface density (see Table 2 of Mousis et al. (2009a) as an illustration of this effect). On the other hand, the composition of planetesimals agglomerated from clathrates depends on the availability of crystalline water at their crystallization epochs. If crystalline water is sufficiently abundant to trap all volatile species in presence, then the composition of the icy phase in planetesimals should also reflect a supersolar abundance of water. For the same reasons as those invoked in the case of pure condensates, the relative mole fractions among the encaged volatiles should slightly depart from protosolar, because of the continuous decrease of the disks surface density at the different epochs of entrapping.

If i) the budget of crystalline water is not significant enough to enable the enclathration of all the volatiles present in the gas phase or ii) the disk temperature never reaches those needed for trapping the most volatile species, then the composition of clathrate must be calculated assuming the simultaneous entrapment of all guests present in the coexisting gas phase. The composition of such multiple guest clathrates is predicted via a statistical thermodynamics approach, based on the van der Waals-Platteeuw statistical theory and the derivation of interaction potential parameters from experimental data (van der Waals and Platteeuw 1959; Lunine and Stevenson 1985; Mousis et al. 2010). These models predict an efficient trapping of CO, H<sub>2</sub>S, Kr and Xe in clathrates at the expense of N<sub>2</sub> and Ar, assuming a PSN protosolar gas. They have been successfully used to interpret the composition of comet 67P/Churyumov-Gerasimenko (hereafter 67P/C-G), which has been found to be substantially depleted in Ar and N<sub>2</sub> compared to the protosolar values by the Rosetta/ ROSINA measurements (Mousis et al. 2016, 2018). One direct consequence of the two aforementioned mechanisms, i.e. condensation and clathration, is that regions where the PSN temperature never reaches extremely low values cannot be populated by ultravolatile-rich planetesimals. The apparent deficiency of Saturn's moon Titan in primordial CO, N<sub>2</sub> and Ar (Niemann et al. 2005) could be thus interpreted as the consequence of its agglomeration of building blocks presenting such deficiencies in ultravolatiles (Hersant et al. 2004; Alibert and Mousis 2007; Mousis et al. 2009b). Figure 5 shows pie charts summarizing the composition of the icy phase incorporated in planetesimals assuming i) the crystallization of pure condensates from a PSN protosolar gas, and ii) the full clathration of volatiles. The case of full clathration of volatiles requires an oxygen abundance that is  $\sim 1.7$  times higher than the protosolar value ( $(\text{O}/\text{H}_2)_{\odot} = 1.21 \times 10^{-3}$ ; Lodders et al. (2009)) for the adopted PSN gas phase mixing ratios ( $\text{CO}:\text{CO}_2:\text{CH}_4 = 10:10:1$  and  $\text{N}_2:\text{NH}_3 = 10$ ).

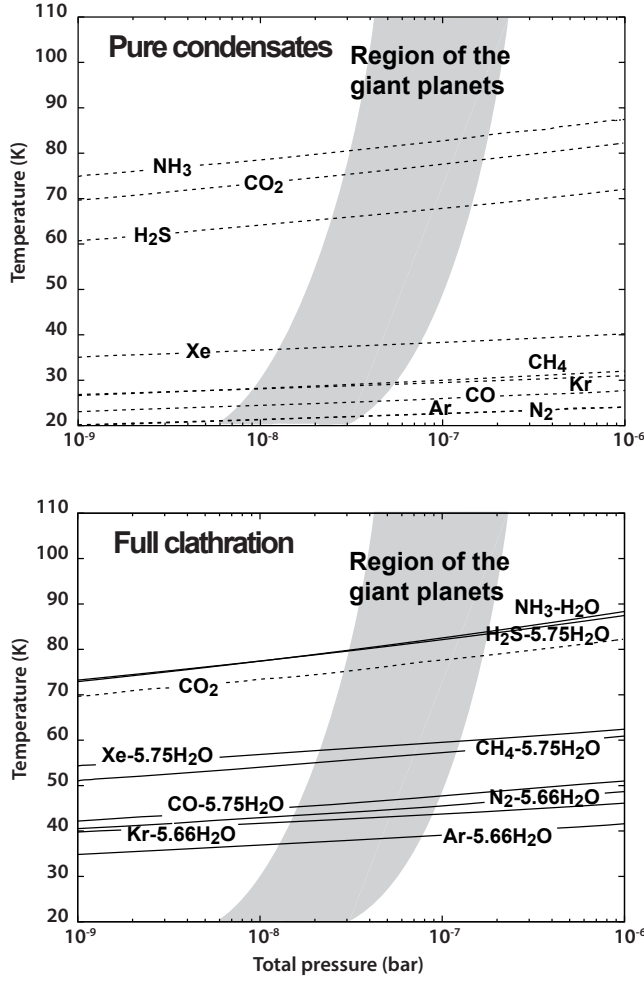


**Fig. 4** Condensation sequence of ices and cooling curve of the PSN in the formation region of the giant planets. Top panel: equilibrium curves of pure condensates (dashed lines), assuming protosolar elemental abundances (Lodders et al. 2009) and  $\text{CO}:\text{CO}_2:\text{CH}_4 = 10:10:1$  and  $\text{N}_2:\text{NH}_3 = 10$  in the gas phase of the disk. Species remain in the gas phase above the equilibrium curves. Bottom panel: same as top panel but in the case of hydrate ( $\text{NH}_3\text{-H}_2\text{O}$ ) and clathrate formation ( $\text{X-5.75H}_2\text{O}$  or  $\text{X-5.67H}_2\text{O}$ ; solid lines), and crystallization of pure  $\text{CO}_2$  condensate (dotted line), assuming a full efficiency of clathration.  $\text{CO}_2$  is the only species that crystallizes at a higher temperature than its associated clathrate in the pressure conditions of the PSN (Mousis et al. 2009a).

### 3.2.3 Desorption of Volatiles at the ACTZ Snowline

In the core accretion model, giant planets grow over a timescale comparable to or longer than nebular thermal evolution. However, planetesimals may migrate radially on much shorter timescales, such that at some point during the growth of core and envelope, planetesimals formed at large distances and thus made of amorphous ice will cross the ACTZ while giant planets are growing (Fig. 6). In this scenario, when particles cross

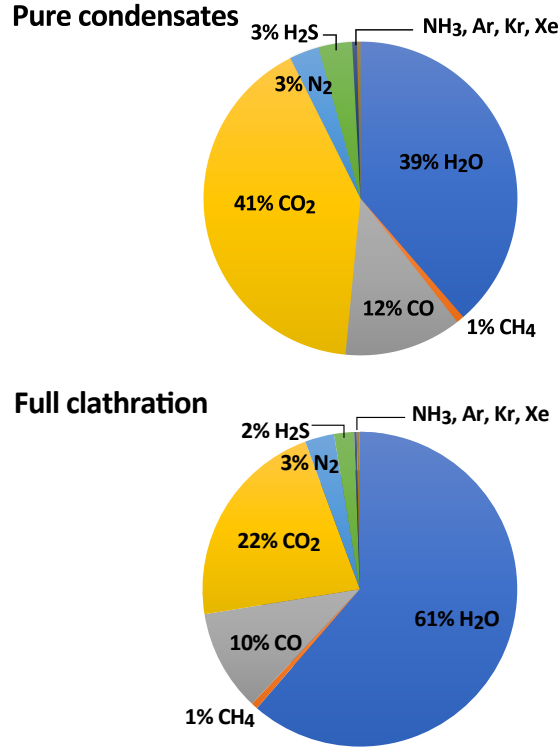


**Fig. 5** Composition of the icy phase incorporated in solids resulting from the agglomeration of pure condensates (top panel) and clathrates (bottom panel). Gas phase and condensation/trapping conditions are those detailed in the caption of Fig. 4.

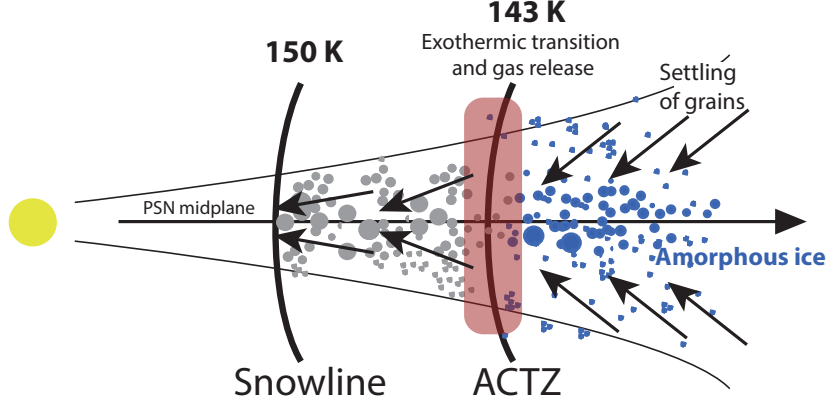


**Fig. 6** Schematic of the relative positions of protoplanetary disk regions where amorphous ice is stable (blue), crystalline ice is present (grey) and then water-vapor only. The dividing lines between the amorphous and crystalline region is the ACTZ, that between ice and vapor is the snowline. Both are temperature-driven. Ice will occur inward of the snowline because inward migration is faster than sublimation for some particle sizes.

the ACTZ, volatiles desorb from amorphous ice and contribute to the disks gas phase (Monga and Desch 2015). The continuous release of vapors by the drifting particles at the location of the ACTZ creates a local enhancement of the gaseous abundances of the released volatiles, compared to their initial values (Mousis et al. 2019). The gas in the region between the ACTZ and snowline is charged with a supersolar abundance of species more volatile than water ice, but not with water vapor. This may provide an explanation for why the gaseous envelope of Jupiter is contaminated with several times solar abundances of heavy noble gases, carbon and nitrogen-bearing species, while the abundance of water from Juno data seems limited to less than twice solar (Wahl et al. 2016). So long as Jupiter formed between the ACTZ and the snowline, it could accrete a gaseous phase enriched in heavy elements except water ice. To limit the accretion of water ice one must then invoke the so-called pebble isolation mass, that of the growing giant planet at which the surrounding gaseous disk is sufficiently perturbed to limit the introduction of small planetesimals (pebbles) in to the giant planet (Bitsch et al. 2018).

If the interplay between gas and solids as outlined above is responsible for the pattern of heavy elements observed in Jupiter, the contribution of this mechanism to the delivery of volatiles to Uranus and Neptune should be very moderate. Figure 7 represents the evolution of the PSN metallicity at different epochs of its evolution. As the disk cools with time, the ACTZ moves inward, and volatiles that are continuously released at the ACTZ diffuse to the outermost regions of the PSN. The figure shows that i) Jupiter’s metallicity is matched over a wide range of distances during the disk evolution, and ii) the disk metallicity drops down to subsolar values at larger heliocentric distances. The abundance of gaseous water is also expected to be by far subsolar since it is located well beyond its corresponding snowline in the formation region of Uranus and Neptune. Figure 8 also illustrates this effect by showing the time evolution of C and O radial profiles in the PSN, assuming that CO and H<sub>2</sub>O are the main carriers of these two elements, and in the case of the inward drift of pure condensates (see Section 3.2.4). Given the fact that these two planets likely formed at the very end of the disk evolution, the abundances of the various gases dropped to even lower values than those reached at earlier epochs in their formation region.

#### 3.2.4 Enhancements of Vapors in the Vicinity of the Pure Condensates Snowlines

PSN gas can also be enriched in heavy elements via the vaporization of pebbles or particles when they cross the snowlines of pure condensates in the 20–40 K range (Booth et al. 2017). The main differences with the ACTZ snowline is the presence of multiple snowlines whose number in the PSN corresponds to that of the considered volatiles and the adding of a sink term related to the condensation of vapors when they diffuse back to their respective snowlines. For the sake of illustration, we present some preliminary calculations based on a disk model whose structure and evolution is ruled by the following second-order differential equation (Lynden-Bell and Pringle 1974):

$$\frac{\partial \Sigma_g}{\partial t} = \frac{3}{r} \frac{\partial}{\partial r} \left[ r^{1/2} \frac{\partial}{\partial r} \left( r^{1/2} \Sigma_g \nu \right) \right]. \quad (1)$$

This equation describes the motion of a viscous accretion disk of surface density  $\Sigma_g$  with radial distance  $r$  and dynamical viscosity  $\nu$ , assuming hydrostatic equilibrium in

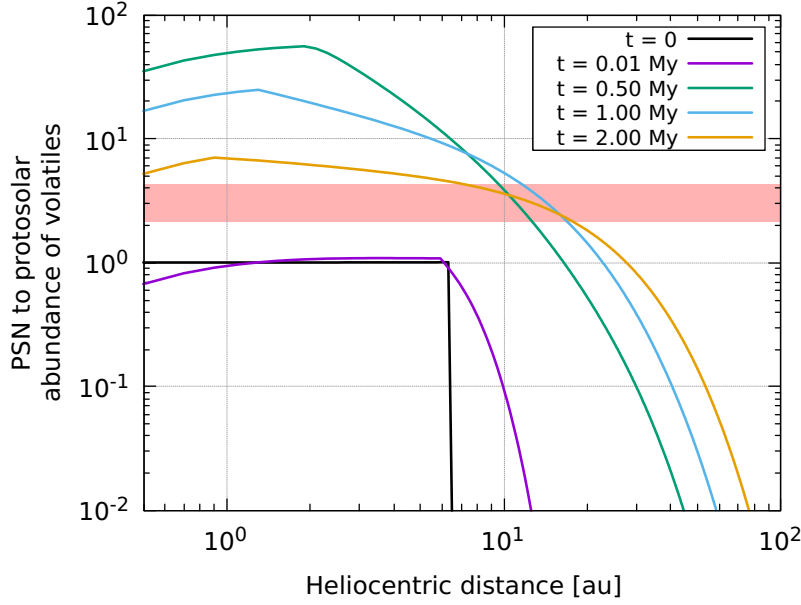


**Fig. 7** Time and radial evolution of the abundances of volatiles released to the PSN gas phase by the icy grains subsequent to their drift through the ACTZ. Calculations have been performed for  $\alpha = 5 \times 10^{-3}$  with the model detailed in Mousis et al. (2019). The horizontal bar represents the range of volatile enrichments (nominal values) measured in Jupiter. With time, the metallicity of the PSN matches Jupiter’s value at decreasing heliocentric distances and becomes progressively subsolar at radii located beyond.

the  $z$  direction, and considering the Sun has reached its final mass of  $1.0 M_{\odot}$ . We use the prescription of Shakura and Sunyaev (1973) for  $\alpha$ -turbulent disks to obtain the gas viscosity  $\nu$ , and the mid-plane temperature  $T_d$  is computed following the approach of Hueso and Guillot (2005). The initial condition is (Lynden-Bell and Pringle 1974):

$$\Sigma_g \nu = \frac{C}{3\pi} \exp\left(-\left(\frac{r}{r_0}\right)^{2-p}\right), \quad (2)$$

where  $C = M_{acc,0}$ , is the mass accretion rate onto the central star at  $r = 0$ , whose value is assumed to be  $10^{-7.6} M_{\odot} \text{ yr}^{-1}$  (Hartmann et al. 1998). We choose  $p = 3/2$ , a value corresponding to an early time disk.  $r_0$  is adjusted to give a starting disk’s mass of  $0.1 M_{\odot}$ . The gas viscosity and midplane temperature are computed at each time step, and the disk is evolved with respect to Eq. 1.

In this study, the  $\text{H}_2$ -He-dominated disk is uniformly filled with  $\text{H}_2\text{O}$  and  $\text{CO}$ , with O and C abundances assumed to be protosolar (Lodders et al. 2009). The condensation temperatures of these two species almost encompass the condensation temperatures of all main volatiles that may be present in the outer PSN (see Fig. 4, top panel). The surface density  $\Sigma_i$  of a trace species  $i$  (for its vapor and solid phase) is numerically evolved, solving the following 1D advection-diffusion equation:

$$\frac{\partial \Sigma_i}{\partial t} + \frac{1}{r} \frac{\partial}{\partial r} \left[ r \left( \Sigma_i v_i - D_i \Sigma_g \frac{\partial}{\partial r} \left( \frac{\Sigma_i}{\Sigma_g} \right) \right) \right] + \dot{Q}_i = 0, \quad (3)$$

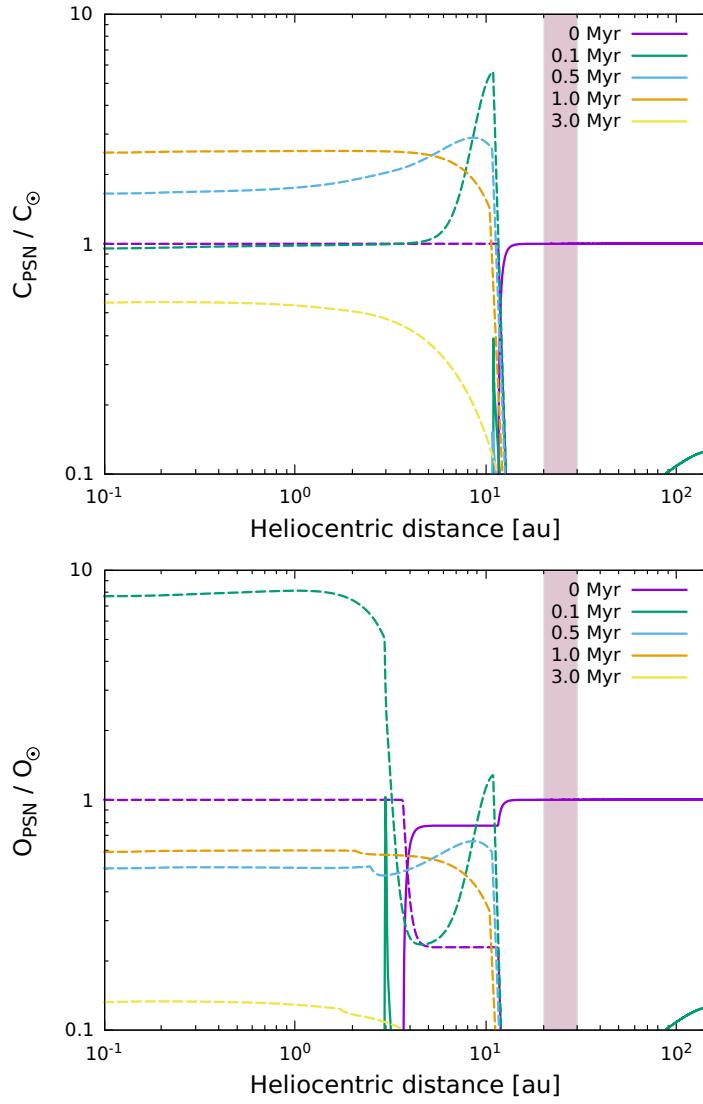
where  $v_i$  and  $D_i$  are the radial velocities and diffusivities of species  $i$ , and  $\dot{Q}_i$  is a source/sink term accounting for sublimation/condensation of vapor  $i$  from solid grains. Vapor properties are those of the PSN gas. Grains' properties are computed using the two-population algorithm detailed in Birnstiel et al. (2012), and we consider that dust grains' dynamical properties are those of the dominant species at each radius. Finally, the evaporation and condensation rates are computed following the approach of Drazkowska and Alibert (2017).

Figure 8 shows that each pure condensate in solid grain form crossing its corresponding snowline sublimates and generates supersolar enrichments for the vapor released at this location. Because the vapor of a given species diffusing outwards re-condenses back into solid grains, this prevents its presence far beyond its snowline. This effect contrasts with the scenario of volatiles released into the PSN when grains cross the ACTZ, and whose vapors cannot be trapped back when volatiles diffuse outward (Fig. 7). After 1 Myr of disk evolution, the gas phase abundances of C- and O-bearing volatiles become substantially subsolar in the outer PSN, indicating that this effect cannot explain the supersolar metallicities measured in Uranus and Neptune. Because Uranus and Neptune likely formed later than this epoch, we find that i) the contrast between our results and the observations becomes reinforced, and ii) this mechanism is even less efficient than the one depicting the delivery of volatiles through the ACTZ.

One should mention that the scenarios of volatiles delivery through the ACTZ (Mousis et al. 2019) or through the different snowlines of pure condensates, as shown in this paper, are based on dynamic models depicting the time evolution of the surface density, radial velocity and temperature radial profiles in the PSN, in contrast with Ali-Dib et al. (2014) and Oberg and Wordsworth (2019) who use static disks. Computing the evolution of the PSN is an important step, since evolution is fast at early times, impacting both dust transport, determined by the PSN density and gas velocity, and thermodynamic conditions, fixed by midplane pressure and temperature.

#### 4 Atmospheric Signatures

Here we use the characteristics of the discussed scenarios of volatiles delivery to derive their corresponding fingerprints in the atmospheres of Uranus and Neptune. To do so, all predictions of the volatile enrichments have been calibrated on the nominal C abundance measured in both planets ( $\sim 80$  times protosolar) (see Sec. 2). Top panel of Fig. 9 represents a homogeneous supersolar enrichment pattern in Uranus and Neptune adjusted to their C abundance measurements. This pattern is valid in the cases of i) volatiles delivered via disk instability, or ii) trapped in amorphous planetesimals, assuming the planets formed via core accretion. Top panel also shows the predictions of subsolar abundances of volatiles delivered by the release of vapors at the location of the ACTZ or at the position of the different snowlines of pure condensates. None of these two scenarios is able to predict the high C enrichment observed in Uranus and Neptune. The upper limits for the subsolar abundances are purely indicative. Much lower values can be obtained as a function of the utilized model, and also by assuming different formation epochs or distances. Bottom panel of Fig. 9 represents



**Fig. 8** Time evolution of radial profiles of C (top panel) and O (bottom panel) in the PSN, normalized to their respective protosolar abundances (Lodders et al. 2009). These two elements are assumed to be distributed between CO and H<sub>2</sub>O who form pure condensates in the outermost regions of the PSN. Solid and dashed lines are used to identify the trace species in solid and gaseous phases, respectively. The vertical purple bars indicate the region of the ice giants in the solar system.

the enrichment patterns of volatiles delivered in solids constituted of clathrates or pure condensates to the two ice giants. These enrichment patterns have been calculated with the model presented in Mousis et al. (2009b) who calculated the volatile enrichments in Jupiter and Saturn as a function of the efficiency of clathration in the PSN. The clathrate case predicts a water abundance in the ice giants that is  $\sim 1.7$  times higher

than the value predicted from the pure condensates scenario (see Sec. 3.2.2). In the clathrate case, the Ar, Kr, Xe, C, N, O, S, and P abundances are predicted to be  $\sim 60, 65, 79, 80, 68, 194, 95,$  and  $87$  times their protosolar abundances, respectively. In the pure condensates case, the Ar, Kr, Xe, C, N, O, S, and P abundances are predicted to be  $\sim 44, 58, 72, 80, 47, 115, 103,$  and  $81$  times their protosolar abundances, respectively. Both cases are adjusted to the C measurement in the ice giants and assume it corresponds to the bulk value measured in the planets.

Our predictions correspond to the assumption that the atmospheres of Uranus and Neptune are homogeneously mixed, and that no compositional gradient exists. This hypothesis is probably simplistic, given the fact that recent interior models suggest the presence of a compositional gradients in those planets (Helled and Bodenheimer 2014; Cavalié et al. 2017; Podolak et al. 2019). However, in absence of a proven mechanism depicting any variation among the relative abundances of heavy elements in the envelopes, the enrichment patterns acquired by the two planets should remain valid, even in the case of compositional gradient. In addition, if the atmospheric signatures result from the volatiles delivery in ices, these latter may have been i) either agglomerated by the ice giants during the growth of their envelopes or ii) accreted with the cores prior to their subsequent releases into the envelopes because of the erosion (Stevenson 1982; Guillot 2004; Wilson and Militzer 2012).

It is difficult to establish a link between planetary migration and the chemical composition of the ice giants. To the best of our knowledge, the only possible test would be the measurement of the noble gas isotopic ratios in the envelopes of ice giants. Since the ESA *Rosetta* spacecraft has measured a non-solar Xe mixture in comet 67P/C-G (Marty et al. 2017), the identification of such a mixture in the atmospheres of the ice giants could tell if their building blocks came from the same formation location as the building blocks of 67P/C-G (see the discussion in Mandt et al. (2020), this issue). These building blocks are supposed to have formed at a very high heliocentric distance in the PSN, may be the highest ever inferred, given the very high D/H ratio measured in the coma of 67P/C-G (Altwegg et al. 2015).

## 5 Conclusions

In this paper, we have investigated what could be the enrichment patterns of several delivery scenarios of the volatiles to the atmospheres of ice giants, having in mind that the only well constrained determination made remotely, i.e. the C abundance measurement, suggests that their envelopes possess highly supersolar metallicities, i.e. close to two orders of magnitude above that of the PSN. In the framework of the core accretion model, only the delivery of volatiles in solid forms (amorphous ice, clathrates, pure condensates) to these planets can account for the apparent supersolar metallicity of their envelopes. In contrast, all mechanisms invoking the delivery of volatiles in vapor forms, because of the inward drift of icy particles through various snowlines, predict subsolar abundances in the envelopes of Uranus and Neptune. Alternatively, even if the disk instability mechanism poses many questions in terms of feasibility in our solar system, it may be consistent with the supersolar metallicities observed in Uranus and Neptune, assuming the two planets suffered subsequent erosion of their H-He envelopes.

Atmospheric entry probes equipped with high-resolution mass spectrometers are the ideal tool to measure the abundances of the main species and their isotopes in the ice



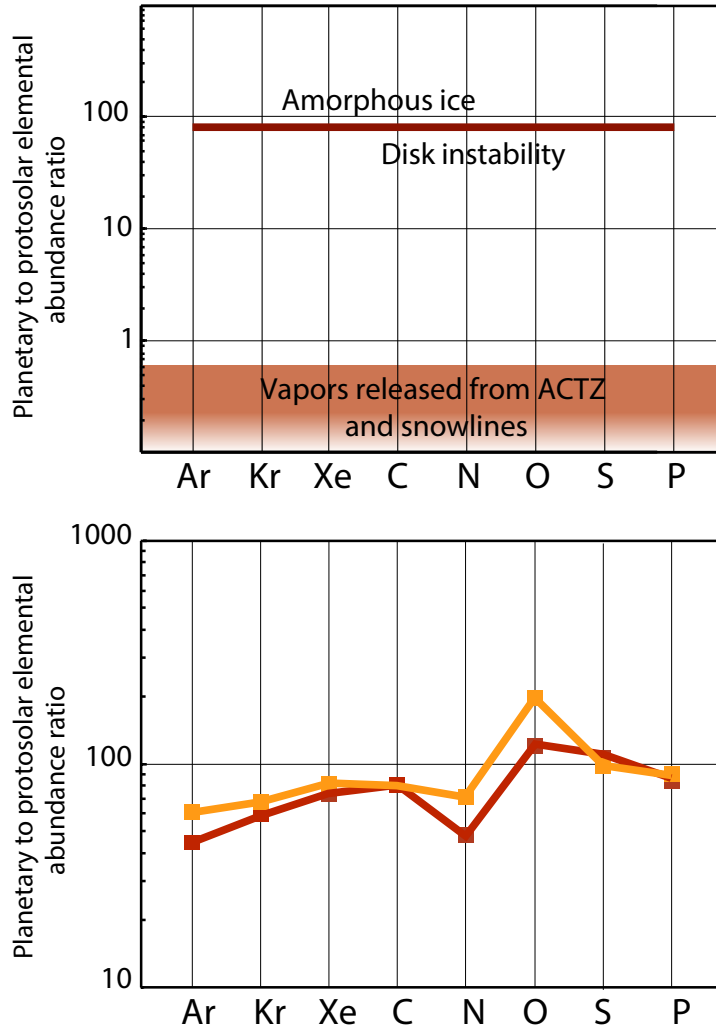


**Fig. 9** Signatures of the different scenarios of volatiles delivery in the envelopes of Uranus and Neptune, assuming homogeneous mixing and that the measured C abundances are representatives of the bulk values. Calibration is done on a C abundance assumed to be 80 times protosolar (see Table 1). *Top panel:* volatiles delivered via disk instability or amorphous planetesimals in the framework of the core accretion model display significant supersolar and homogeneous volatiles enrichments, compared to their protosolar abundances. Volatiles delivered as vapors desorbed from the ACTZ or resulting from the sublimation of pure condensates at their respective snowlines display subsolar abundances in the envelopes. *Bottom panel:* atmospheric signatures of volatiles accreted in the ice giants in forms of pure condensates (red lines) or clathrates (orange lines).

giants, given the difficulty of remotely sounding the atmospheres down to the different condensation levels. We refer the reader to the works of Atreya et al. (2020) and Atkinson et al. (2020), this issue, for thorough discussions about the depths that can be sampled by a probe or an orbiter as a function of the science objectives. Interestingly, subsequent probe measurements should focus on the determination of the abundances of the heavy noble gases since these latter never condense in the envelopes of Uranus and Neptune and are therefore well mixed, even in the top layers at the  $\sim 1$ -bar level. The trapping properties of noble gases in various icy materials are fairly well known, thanks to laboratory experiments. For example, heavy noble gases are efficiently adsorbed on amorphous ice (Bar-Nun et al. 2007) while Ar is a poor clathrate former because of its small atomic size (Sloan and Koh 2008). The resulting Xe/Ar ratio that desorbed from amorphous ice should then be roughly protosolar in the envelopes of ice giants. In contrast, the same ratio released from clathrates is expected to be supersolar in these envelopes. Also, if the envelopes of the ice giants formed from vapors released at various snowlines instead of a mixture of gas and solids, the abundances of heavy noble gases should be subsolar in their atmospheres. This trend severely departs from the supersolar abundances predicted in the cases corresponding to full clathration or condensation of volatiles in the giant planets' feeding zones. In other words, because noble gases are highly sensitive to the considered mechanism of volatiles delivery, resulting in relative abundances that significantly depend on the delivery process, they should be considered as the top priority of the measurements to be made by an ice giant entry probe.

**Acknowledgements** O.M. and T. C. acknowledge support from CNES. J.I.L. was supported by the Juno project. K.E.M. acknowledges support from the Rosetta project through JPL subcontract 1585002 and by NASA RDAP grant 80NSSC19K1306. We thank the two anonymous reviewers for their useful comments.

## References

- Ali-Dib, M., Mousis, O., Petit, J.-M., Lunine, J. I. 2014. Carbon-rich Planet Formation in a Solar Composition Disk. *The Astrophysical Journal* 785, 125.
- Alibert, Y., Mousis, O. 2007. Formation of Titan in Saturn's subnebula: constraints from Huygens probe measurements. *Astronomy and Astrophysics* 465, 1051.
- Altwegg, K., and 31 colleagues 2015. 67P/Churyumov-Gerasimenko, a Jupiter family comet with a high D/H ratio. *Science* 347, 1261952.
- Armitage, P. J. 2010. Astrophysics of Planet Formation. *Cambridge University Press*, 284pp.
- Asplund, M., Grevesse, N., Sauval, A. J., Scott, P. 2009. The Chemical Composition of the Sun. *Annual Review of Astronomy and Astrophysics* 47, 481.
- Atkinson, D.H., Mousis, O., Spilker, T.R., and Ferri, F. 2020. Model payload for ice giant entry probe missions. *Space Science Reviews*, submitted.
- Atreya, S.K., Hofstadter, M.H., In, J.H., Mousis, O., Reh, K., and Wong, M.H. 2020. Deep Atmosphere Composition, Structure, Origin, and Exploration, with Particular Focus on Critical in situ Science at the Icy Giants. *Space Science Reviews* 216, 18. <https://doi.org/10.1007/s11214-020-0640-8>
- Atreya, S.K., Crida, A., Guillot, T., Lunine, J.I., Madhusudhan, N., and Mousis, O. 2019. The origin and evolution of Saturn, with exoplanet perspective. In *Saturn in the 21st Century*, (eds. K. Baines, M. Flasar, N. Krupp, and T. Stallard), *Cambridge University Press*, pp5–43.
- Bar-Nun, A., Notesco, G., Owen, T. 2007. Trapping of N<sub>2</sub>, CO and Ar in amorphous ice—Application to comets. *Icarus* 190, 655.
- Birnstiel, T., Klahr, H., Ercolano, B. 2012. A simple model for the evolution of the dust population in protoplanetary disks. *Astronomy and Astrophysics* 539, A148.

- Bitsch, B., Morbidelli, A., Johansen, A., Lega, E., Lambrechts, M., Crida, A. 2018. Pebble-isolation mass: Scaling law and implications for the formation of super-Earths and gas giants. *Astronomy and Astrophysics* 612, A30.
- Boley, A. C., Helled, R., Payne, M. J. 2011. The Heavy-element Composition of Disk Instability Planets Can Range from Sub- to Super-nebular. *The Astrophysical Journal* 735, 30.
- Booth, R. A., Clarke, C. J., Madhusudhan, N., Ilee, J. D. 2017. Chemical enrichment of giant planets and discs due to pebble drift. *Monthly Notices of the Royal Astronomical Society* 469, 3994.
- Boss, A. P. 1997. Giant planet formation by gravitational instability. *Science* 276, 1836.
- Brouwers, M. G., Vazan, A., Ormel, C. W. 2018. How cores grow by pebble accretion. I. Direct core growth. *Astronomy and Astrophysics* 611, A65.
- Cavalié, T., Venot, O., Selsis, F., Hersant, F., Hartogh, P., Leconte, J. 2017. Thermochemistry and vertical mixing in the tropospheres of Uranus and Neptune: How convection inhibition can affect the derivation of deep oxygen abundances. *Icarus* 291, 1.
- Chambers, J. 2017. Steamworlds: Atmospheric Structure and Critical Mass of Planets Accreting Icy Pebbles. *The Astrophysical Journal* 849, 30.
- Choukroun, M., Vu, T. H., Fayolle, E. C. 2019. No compelling evidence for clathrate hydrate formation under interstellar medium conditions over laboratory time scales. *Proceedings of the National Academy of Science* 116, 14407.
- Cyr, K. E., Sharp, C. M., Lunine, J. I. 1999. Effects of the redistribution of water in the solar nebula on nebular chemistry. *Journal of Geophysical Research* 104, 19003.
- Cyr, K. E., Sears, W. D., Lunine, J. I. 1998. Distribution and Evolution of Water Ice in the Solar Nebula: Implications for Solar System Body Formation. *Icarus* 135, 537.
- Drazkowska, J., Alibert, Y. 2017. Planetesimal formation starts at the snow line. *Astronomy and Astrophysics* 608, A92.
- Encrenaz, T. 2000. Infrared remote sensing of planetary atmospheres. *Academie des Sciences Paris Comptes Rendus Serie Physique Astrophysique* 1, 1245.
- Feuchtruber, H., and 11 colleagues 2013. The D/H ratio in the atmospheres of Uranus and Neptune from Herschel-PACS observations. *Astronomy and Astrophysics* 551, A126.
- Fletcher, L. N., de Pater, I., Orton, G. S., Hammel, H. B., Sitko, M. L., Irwin, P. G. J. 2014. Neptune at summer solstice: Zonal mean temperatures from ground-based observations, 2003-2007. *Icarus* 231, 146.
- Fletcher, L. N., Drossart, P., Burgdorf, M., Orton, G. S., Encrenaz, T. 2010. Neptune's atmospheric composition from AKARI infrared spectroscopy. *Astronomy and Astrophysics* 514, A17.
- Gautier, D., Hersant, F., Mousis, O., Lunine, J. I. 2001. Enrichments in Volatiles in Jupiter: A New Interpretation of the Galileo Measurements. *The Astrophysical Journal* 550, L227.
- Gautier, D., Conrath, B. J., Owen, T., de Pater, I., Atreya, S. K. 1995. The troposphere of Neptune. *Neptune and Triton* 547.
- Ghosh, J., and 6 colleagues 2019b. Reply to Choukroun et al.: IR and TPD data suggest the formation of clathrate hydrates in laboratory experiments simulating ISM. *Proceedings of the National Academy of Science* 116, 14409.
- Ghosh, J., and 6 colleagues 2019a. Clathrate hydrates in interstellar environment. *Proceedings of the National Academy of Science* 116, 1526.
- Guillot, T. 2004. Probing the giant planets. *Physics Today* 57, 4.63.
- Gulkis, S., Janssen, M. A., Olsen, E. T. 1978. Evidence for the depletion of ammonia in the Uranus atmosphere. *Icarus* 34, 10.
- Hartmann, L., Calvet, N., Gullbring, E., D'Alessio, P. 1998. Accretion and the Evolution of T Tauri Disks. *The Astrophysical Journal* 495, 385.
- Helled, R., Bodenheimer, P. 2014. The Formation of Uranus and Neptune: Challenges and Implications for Intermediate-mass Exoplanets. *The Astrophysical Journal* 789, 69.
- Helled, R., Anderson, J. D., Podolak, M., Schubert, G. 2011. Interior Models of Uranus and Neptune. *The Astrophysical Journal* 726, 15.
- Hersant, F., Gautier, D., Lunine, J. I. 2004. Enrichment in volatiles in the giant planets of the Solar System. *Planetary and Space Science* 52, 623.
- Hueso, R., Guillot, T. 2005. Evolution of protoplanetary disks: constraints from DM Tauri and GM Aurigae. *Astronomy and Astrophysics* 442, 703.
- Izidoro, A., Morbidelli, A., Raymond, S. N., Hersant, F., Pierens, A. 2015. Accretion of Uranus and Neptune from inward-migrating planetary embryos blocked by Jupiter and Saturn. *Astronomy and Astrophysics* 582, A99.

- Irwin, P. G. J., and 7 colleagues 2019b. Latitudinal variation in the abundance of methane ( $\text{CH}_4$ ) above the clouds in Neptune's atmosphere from VLT/MUSE Narrow Field Mode Observations. *Icarus* 331, 69.
- Irwin, P. G. J., and 6 colleagues 2019a. Probable detection of hydrogen sulphide ( $\text{H}_2\text{S}$ ) in Neptune's atmosphere. *Icarus* 321, 550.
- Irwin, P. G. J., and 6 colleagues 2018. Detection of hydrogen sulfide above the clouds in Uranus's atmosphere. *Nature Astronomy* 2, 420.
- Karkoschka, E., Tomasko, M. G. 2011. The haze and methane distributions on Neptune from HST-STIS spectroscopy. *Icarus* 211, 780.
- Karkoschka, E., Tomasko, M. 2009. The haze and methane distributions on Uranus from HST-STIS spectroscopy. *Icarus* 202, 287.
- Lambrechts, M., Johansen, A. 2014. Forming the cores of giant planets from the radial pebble flux in protoplanetary discs. *Astronomy and Astrophysics* 572, A107.
- Lambrechts, M., Johansen, A., Morbidelli, A. 2014. Separating gas-giant and ice-giant planets by halting pebble accretion. *Astronomy and Astrophysics* 572, A35.
- Lambrechts, M., Johansen, A. 2012. Rapid growth of gas-giant cores by pebble accretion. *Astronomy and Astrophysics* 544, A32.
- Lellouch, E., and 8 colleagues 2015. New constraints on the  $\text{CH}_4$  vertical profile in Uranus and Neptune from Herschel observations. *Astronomy and Astrophysics* 579, A121.
- Lellouch, E., and 53 colleagues 2010. First results of Herschel-PACS observations of Neptune. *Astronomy and Astrophysics* 518, L152.
- Levison, H. F., Duncan, M. J., Brasser, R., Kaufmann, D. E. 2010. Capture of the Sun's Oort Cloud from Stars in Its Birth Cluster. *Science* 329, 187.
- Levison, H. F., Morbidelli, A. 2007. Models of the collisional damping scenario for ice-giant planets and Kuiper belt formation. *Icarus* 189, 196.
- Lindal, G. F. 1992. The Atmosphere of Neptune: an Analysis of Radio Occultation Data Acquired with Voyager 2. *The Astronomical Journal* 103, 967.
- Lindal, G. F., Lyons, J. R., Sweetnam, D. N., Eshleman, V. R., Hinson, D. P., Tyler, G. L. 1987. The atmosphere of Uranus: Results of radio occultation measurements with Voyager 2. *Journal of Geophysical Research* 92, 14987.
- Liu, S.-F., and 6 colleagues 2019. The formation of Jupiter's diluted core by a giant impact. *Nature* 572, 355.
- Lynden-Bell, D., Pringle, J. E. 1974. The evolution of viscous discs and the origin of the nebular variables. *Monthly Notices of the Royal Astronomical Society* 168, 603.
- Lodders, K., Palme, H., Gail, H.-P. 2009. Abundances of the Elements in the Solar System. Landolt-Börnstein 4B, 712.
- Lozovsky, M., Helled, R., Rosenberg, E. D., Bodenheimer, P. 2017. Jupiter's Formation and Its Primordial Internal Structure. *The Astrophysical Journal* 836, 227.
- Lunine, J. I., Stevenson, D. J. 1985. Thermodynamics of clathrate hydrate at low and high pressures with application to the outer solar system. *The Astrophysical Journal Supplement Series* 58, 493.
- Mandt, K.E., Mousis, O., Lunine, J.I., Marty, B., Smith, T., Luspai-Kuti, A., and Aguichine, A. Tracing the Origins of the Ice Giants through Noble Gas Isotopic Composition. *Space Science Reviews*, submitted.
- Mandt, K. E., Mousis, O., Treat, S 2019. Applying Rosetta noble gas abundances and xenon isotopes to determine the origin of the building blocks of the ice giants. *Monthly Notices of the Royal Astronomical Society* 491(1), 488-494.
- Mandt, K. E., and 6 colleagues 2015. Constraints from Comets on the Formation and Volatile Acquisition of the Planets and Satellites. *Space Science Reviews* 197, 297.
- Marty, B., and 29 colleagues 2017. Xenon isotopes in 67P/Churyumov-Gerasimenko show that comets contributed to Earth's atmosphere. *Science* 356, 1069.
- Mayer, L., Quinn, T., Wadsley, J., Stadel, J. 2004. The Evolution of Gravitationally Unstable Protoplanetary Disks: Fragmentation and Possible Giant Planet Formation. *The Astrophysical Journal* 609, 1045.
- Monga, N., Desch, S. 2015. External Photoevaporation of the Solar Nebula: Jupiter's Noble Gas Enrichments. *The Astrophysical Journal* 798, 9.
- Morbidelli, A., Tsiganis, K., Batygin, K., Crida, A., Gomes, R. 2012. Explaining why the uranian satellites have equatorial prograde orbits despite the large planetary obliquity. *Icarus* 219, 737.

- Mousis, O., Ronnet, T., Lunine, J. I. 2019. Jupiter's Formation in the Vicinity of the Amorphous Ice Snowline. *The Astrophysical Journal* 875, 9.
- Mousis, O., and 10 colleagues 2018. Noble Gas Abundance Ratios Indicate the Agglomeration of 67P/Churyumov-Gerasimenko from Warmed-up Ice. *The Astrophysical Journal* 865, L11.
- Mousis, O., and 12 colleagues 2016. A Protosolar Nebula Origin for the Ices Agglomerated by Comet 67P/Churyumov-Gerasimenko. *The Astrophysical Journal* 819, L33.
- Mousis, O., Lunine, J. I., Picaud, S., Cordier, D. 2010. Volatile inventories in clathrate hydrates formed in the primordial nebula. *Faraday Discussions* 147, 509.
- Mousis, O., and 7 colleagues 2009b. Determination of the Minimum Masses of Heavy Elements in the Envelopes of Jupiter and Saturn. *The Astrophysical Journal* 696, 1348.
- Mousis, O., and 10 colleagues 2009a. Clathration of Volatiles in the Solar Nebula and Implications for the Origin of Titan's Atmosphere. *The Astrophysical Journal* 691, 1780.
- Niemann, H. B., and 17 colleagues 2005. The abundances of constituents of Titan's atmosphere from the GCMS instrument on the Huygens probe. *Nature* 438, 779.
- Öberg, K. I., Wordsworth, R. 2019. Jupiter's composition suggests its core assembled exterior to the N<sub>2</sub> snowline. *The Astronomical Journal* 158, 194.
- Orton, G. S., and 9 colleagues 2014b. Mid-infrared spectroscopy of Uranus from the Spitzer Infrared Spectrometer: 1. Determination of the mean temperature structure of the upper troposphere and stratosphere. *Icarus* 243, 494.
- Orton, G. S., and 9 colleagues 2014a. Mid-infrared spectroscopy of Uranus from the Spitzer infrared spectrometer: 2. Determination of the mean composition of the upper troposphere and stratosphere. *Icarus* 243, 471.
- Owen, T., and 6 colleagues 1999. A low-temperature origin for the planetesimals that formed Jupiter. *Nature* 402, 269.
- de Pater, I., Romani, P. N., Atreya, S. K. 1991. Possible microwave absorption by H<sub>2</sub>S gas in Uranus' and Neptune's atmospheres. *Icarus* 91, 220.
- de Pater, I., Romani, P. N., Atreya, S. K. 1989. Uranus deep atmosphere revealed. *Icarus* 82, 288.
- Pepin, R. O. 1991. On the origin and early evolution of terrestrial planet atmospheres and meteoritic volatiles. *Icarus* 92, 2.
- Podolak, M., Helled, R., Schubert, G. 2019. Effect of non-adiabatic thermal profiles on the inferred compositions of Uranus and Neptune. *Monthly Notices of the Royal Astronomical Society* 487, 2653.
- Podolak, M., Pollack, J. B., Reynolds, R. T. 1988. Interactions of planetesimals with protoplanetary atmospheres. *Icarus* 73, 163.
- Pollack, J. B., Hubickyj, O., Bodenheimer, P., Lissauer, J. J., Podolak, M., Greenzweig, Y. 1996. Formation of the Giant Planets by Concurrent Accretion of Solids and Gas. *Icarus* 124, 62.
- Reinhardt, C., Chau, A., Stadel, J., Helled, R. 2019. Bifurcation in the history of Uranus and Neptune: the role of giant impacts. arXiv e-prints arXiv:1907.09809.
- Ros, K., Johansen, A. 2013. Ice condensation as a planet formation mechanism. *Astronomy and Astrophysics* 552, A137.
- Rubin, M., and 31 colleagues 2015. Molecular nitrogen in comet 67P/Churyumov-Gerasimenko indicates a low formation temperature. *Science* 348, 232.
- Schmitt, B., Espinasse, S., Grim, R. J. A., Greenberg, J. M., Klinger, J. 1989. Laboratory studies of cometary ice analogues. *Physics and Mechanics of Cometary Materials, ESA Special Publication* 65.
- Shakura, N. I., Sunyaev, R. A. 1973. Black holes in binary systems. Observational appearance. *Astronomy and Astrophysics* 500, 33.
- Simon, A.A., Fletcher, L.N., Arridge, C. et al. 2020. A Review of the in Situ Probe Designs from Recent Ice Giant Mission Concept Studies. *Space Science Reviews* 216, 17. <https://doi.org/10.1007/s11214-020-0639-1>
- Sloan, E.D., Koh, C.A. 2008. Clathrate Hydrates of Natural Gases, third ed. *CRC Press, Taylor & Francis Group, Boca Raton*.
- Smith, B. A., and 64 colleagues 1989. Voyager 2 at Neptune: Imaging Science Results. *Science* 246, 1422.
- Smith, B. A., and 39 colleagues 1986. Voyager 2 in the Uranian System: Imaging Science Results. *Science* 233, 43.

- 
- Stevenson, D. J., Lunine, J. I. 1988. Rapid formation of Jupiter by diffusive redistribution of water vapor in the solar nebula. *Icarus* 75, 146.
- Stevenson, D. J. 1982. Formation of the giant planets. *Planetary and Space Science* 30, 755.
- Sromovsky, L. A., Karkoschka, E., Fry, P. M., Hammel, H. B., de Pater, I., Rages, K. 2014. Methane depletion in both polar regions of Uranus inferred from HST/STIS and Keck/NIRC2 observations. *Icarus* 238, 137.
- Sromovsky, L. A., Fry, P. M., Kim, J. H. 2011. Methane on Uranus: The case for a compact CH<sub>4</sub> cloud layer at low latitudes and a severe CH<sub>4</sub> depletion at high-latitudes based on re-analysis of Voyager occultation measurements and STIS spectroscopy. *Icarus* 215, 292.
- Stone, E. C., Miner, E. D. 1989. The Voyager 2 Encounter with the Neptunian System. *Science* 246, 1417.
- Stone, E. C., Miner, E. D. 1986. The Voyager 2 Encounter with the Uranian System. *Science* 233, 39.
- Tyler, G. L., and 9 colleagues 1986. Voyager 2 Radio Science Observations of the Uranian System: Atmosphere, Rings, and Satellites. *Science* 233, 79.
- van der Waals, J.H., Platteeuw, J.C. 1959. Clathrate solutions. *Advances in Chemical Physics*, vol. 2. *Interscience, New York*, pp. 157.
- Wahl, S. M., Hubbard, W. B., Militzer, B. 2016. Tidal Response of Preliminary Jupiter Model. *The Astrophysical Journal* 831, 14.
- Wilson, H. F., Militzer, B. 2012. Solubility of Water Ice in Metallic Hydrogen: Consequences for Core Erosion in Gas Giant Planets. *The Astrophysical Journal* 745, 54.